Advanced Steel Construction – Vol. 20 No. 4 (2024) 319–329
DOI:10.18057/IJASC.2024.20.4.1

EXPERIMENTAL AND FINITE ELEMENT INVESTIGATIONS OF CONCRETE-FILLED STEEL SLENDER COLUMNS WITH HEXAGONAL CROSS-SECTION

O. F. Kharoob, M. H. EL-Boghdadi and AZA. M. Elagamey *

Department of Structural Engineering, Faculty of Engineering, Tanta University, Tanta, Egypt
** (Corresponding author: E-mail: aza_mohamed@yahoo.com)*

ABSTRACT

This research presents experimental and finite element (FE) investigations of hexagonal concrete-filled steel tubular (HCFST) slender columns. Firstly, a uniform axial load is applied to eight HCFST columns, with four of them being short columns and the others remainder slender. The experiments aim to study the impact of both the cross-section and concrete strength on the strength and behavior of HCFST slender columns. Secondly, HCFST slender columns are analyzed using the FE program (ABAQUS). Validation of the FE analysis in terms of strength and behavior is conducted using the present experimental tests and previous research. The strength and behavior of HCFST slender columns are further explored using a series of parametric studies, including columns' height, concrete strength (f_c), steel cross-section thickness (t), and steel strength (f_y). The results show that increasing the values of t, f_c, and f_y increases the ultimate capacity load of HCFST slender columns. Additionally, the maximum value of λ is identified to be almost equal to 18, indicating the threshold distinguishing short HCFST columns, and after this threshold, the columns are classified as slender. Lastly, a comparison is drawn between the results obtained from the experimental and FE models and the standards obtained in the AISC and EN 1994-1-1 (EC4) codes. The analysis reveals that EN 1994-1-1 (EC4) yields non-conservative results for steel tubes with small thicknesses, whereas AISC tends to give more conservative results across all HCFST slender columns. It is therefore recommended to adhere to the AISC specification for steel tubes with small thicknesses up to 4mm and to use EC4 for other thicknesses exceeding this limit.

ARTICLE HISTORY

Received: 21 August 2023
Revised: 11 February 2024
Accepted: 16 February 2024

KEYWORDS

HCFST slender columns;
Ultimate axial strength;
Experimental study;
Slenderness ratio;
Finite element (FE)

Copyright © 2024 by The Hong Kong Institute of Steel Construction. All rights reserved.

1. Introduction

Generally, composite columns consist of concrete as the compression element, while steel members at the external perimeter are considered the best elements to withstand tension and bending moments. The presence of the concrete component within the steel tube effectively mitigates local buckling by providing resistance compressive loading. Concrete-filled steel tubing (CFST) columns have found extensive application in various structures such as transmission towers, bridges, multi-story buildings, and storerooms. As depicted in Fig. 1, the shapes of CFST columns include rectangular, square, circular, elliptical, and more recently, octagonal and hexagonal shapes. The main advantages of using CFST columns were: economy, increased strength, greater ductility, higher stiffness, higher energy absorption capacity, and reduced construction time and cost [1].

Circular CFST columns perform significantly better than their square or rectangular counterparts due to the more uniform confinement effect experienced by a circular CFST column than on a square or rectangular cross-section [2]. The cross-sections of CFST columns can vary, encompassing shapes such as octagonal [3–6], hexagonal [1, 7–10], round-ended [11–14], and elliptical [15–19] shapes. These shapes have been extensively studied to enhance bearing capacity and simplify connections to neighboring beams.

A new cross-section for CFST columns, termed square concrete-filled double steel tubular (CFDST) columns, has been introduced. This design incorporates an inner circular tube, aiming to combine the advantages of square and circular CFST columns, as described in references [3, 20]. Researchers have tested square CFDST columns under various loads to assess their structural performance [21–25].

Conversely, slender columns have been extensively studied, including circular, square, and oval specimens. Dundu [26] examined the behavior of 29 squares of CFST under concentric axial compression. Overall, buckling was identified as the predominant failure mode for column lengths ranging between 1.5 and 2.7 m. Dai et al. [27] conducted numerical forecasts in conjunction with experimental observations of 18 CFST elliptical columns, verifying the accuracy of the FE. The failure mechanisms observed in the slender CFST columns were global buckling, as established through both experimental and numerical modeling. Ahmed et al. [28] studied numerical models to identify local and global buckling in CFDST columns, proposing a design methodology for calculating the ultimate load. Wang et al. [29] conducted tests on 13 HCFS corner columns under axial or eccentric compression, proposing equations to predict load capacity and providing insights for safe design predictions.

According to the aforementioned, previous studies concentrated on studying the behavior of short CFST columns, with very limited investigation into CFST slender columns with oval, circular, and square cross-sections. However, it is worth noting that there was limited availability of experimental or theoretical investigations regarding the behavior of CFST slender columns with hexagonal cross-sections, except for the findings presented in reference [29].

Recently, only one study has appeared examining slender columns of hexagonal cross-section subjected to eccentric compression [29].

Therefore, the authors believed that this research would complete the study of the behavior of slender columns with a hexagonal cross-section using practical experiments exposed to an axial load. At the end of the experimental study, the ABAQUS program was used to develop the FE model. The FE model was verified by using the results of experiments. Then, the proposed FE model was used in the parametric study, which examined the impacts of column height (H), steel cross-section thickness (t), concrete strength (f_c), steel strength (f_y), and slenderness ratio (λ) on the efficiency of HCFST slender columns. Finally, the results of the FE model study and experimental tests were compared with the guidelines outlined in the AISC and EN 1994-1-1 (EC4) codes.

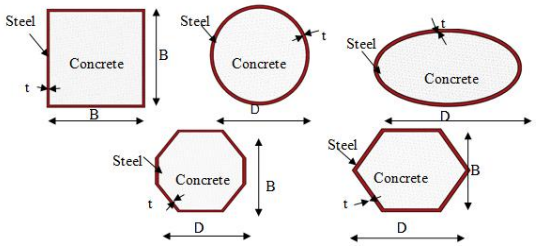

Fig. 1 Shapes of CFST columns

2. Laboratory investigation

2.1. Stage of pre-loading

CFST columns with hexagonal shapes were tested. The experimental program contained eight test specimens of HCFST columns, including four specimens of HCFST short columns (HCSS1, HCSS2, HCSS3, and HCSS4) and four specimens of HCFST slender columns (HCFST1, HCFST2, HCFST3, and HCFST4). The dimensions of tested columns were represented as [$D \times B \times$

t], with the height denoted as [*H*], (θ) of the cross-section 120º, and the calculated value a = *D/2*, with the steel column's thickness [*t*]; please refer to Table 1. Definitions for (*B*, *D*, θ, and a) were provided in Fig. 2. Additionally, Table 1 presents the peak axial strength ($P_{ul,Test}$) of tested columns. The concrete had a strength of 30.25 MPa. Steel plates were bent to create the hexagonal steel tubes, which were then butt-welded at the corners of both ends. Fig. 2 depicts the location of the butt welds along the column length. To monitor the failure mode and prevent rusting of the steel outer surface, the exterior of the steel columns' was treated and painted with gray paint. Initially, the end bearing plate and hexagonal steel tube were welded together. Then, concrete was cast from the other side of the columns. The upper surface of the concrete was leveled to be on the same surface plane as the steel column. Concurrently, the standard concrete cube tests were performed.

After casting, the columns were covered with wet burlap on the upper surfaces to prevent water loss. The top surfaces of the columns were regularly watered. Additionally, the standard concrete cubes were treated in a similar manner as the HCFST columns.

Finally, the other side of the column was covered with plates that were welded to the higher surfaces of the HCFST columns.

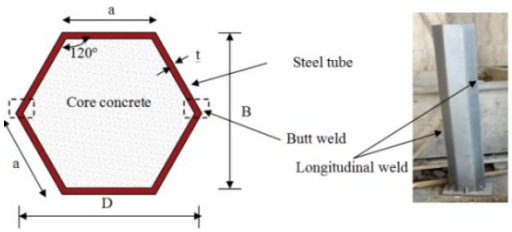

Fig. 2 Definition of symbols and position of butt weld for HCFST columns

Table 1
Tested columns' measurements and ultimate loads

Specimen	*a*[mm]	*H*[mm]	*D*[mm]	*B*[mm]	*t*[mm]	*θ*	P_{uExp}[KN]
HCSS1	80	500	160	138.56	3	120º	894.54
HCSS2	80	500	160	138.56	3	120º	868.53
HCSS3	100	620	200	173.21	3	120º	1178.61
HCSS4	100	620	200	173.21	3	120º	1388.73
HCFST1	80	1494	160	138.56	3	120º	771.63
HCFST2	100	1494	200	173.21	3	120º	1023.57
HCFST3	80	1094	160	138.56	3	120º	879.75
HCFST4	100	1094	200	173.21	3	120º	1100.07

2.2. Stage measurements and loading

The concrete mix specifications are detailed in Table 2. Prior to testing, the mechanical properties of both steel and concrete cubes were examined using standard methods. Concrete cubes measuring 150mm x 150mm x 150mm underwent compression testing according to the procedures outlined in the Egyptian Code [30]. The recorded results of cubic strength [f_{cu}], Young's modulus of the concrete [E_c], and Poison's ratio [v_c] were presented in Table 3. The coupon dimensions of steel plates, corresponding to the Australian Standard AS 1391 [31], were depicted in Figs. 3 and 4. Fig. 5 illustrates the mode of failure observed in the tested plate. The results of the material properties of the steel plates' yield strength [f_y], tensile strengths [f_u], Young's modulus [E_s], and Poison's ratio [v_s] were listed in Table 4 and plotted in Fig. 6. A hydraulic machine applied a 2000 kN axial compression to the test column. The column was stabilized to ensure that the applied load acted uniformly as axial compression. To prevent out-of-plane buckling, a transverse beam was used at mid-height. The two-end boundary conditions of the columns were depicted as hinged supports, as depicted in Fig. 7. To ensure accurate measurement of deformation, four mechanical LVDTs were positioned: two for measuring axial shortening and the others for measuring lateral displacement of the columns', as outlined in Figs. 7 and 8. Additionally, four strain gauges were installed at the midpoint of the two opposing side surfaces of steel tube for the slender columns made of hexagonal concrete-filled steel tubing (HCFST). At the midpoint of the columns' height, strain gauges were positioned: two in tension and two in compression, one vertically and the other horizontally. The axial load was acted upon the upper surface of the rigid steel plate by a hydraulic cylinder in increments of 20 kN up to 30% of the design load and then unloaded. Subsequently, the load was gradually applied until failure was observed. With every increase in load, readings from the strain gauges and LVDTs were recorded.

Table 2
Concrete mix design

Cement[Kg/m^3]	Water[Kg/m^3]	Sand[Kg/m^3]	Aggregate[Kg/m^3]
350	150	650	1300

Table 3
Properties of concrete

f_{cu} [Mpa]	E_c [Mpa]	v_c
30.25	22970.76	0.23

Fig. 3 Tensile coupon test specimen setup

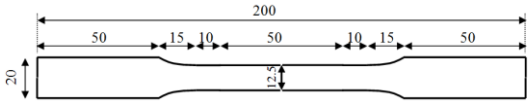

Fig. 4 Dimensions of the test specimen for tensile coupons in mm [31]

Fig. 5 Failure mode of tensile coupon test specimen

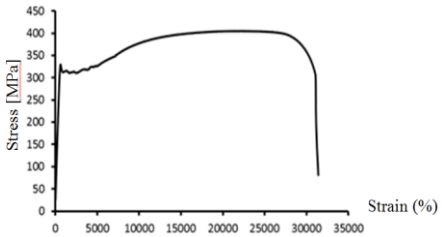

Fig. 6 Steels stress-strain curve

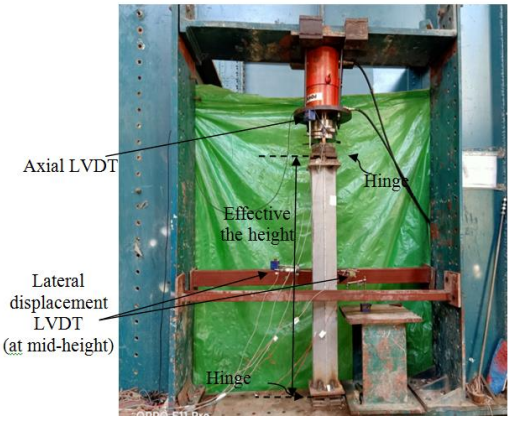

Fig. 7 Test set-up of test specimens

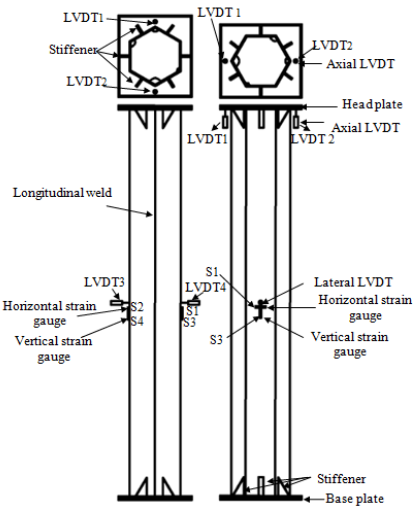

Fig. 8 Strain gauges and LVDTs on the slender columns

Table 4
Measured steel properties

f_y [Mpa]	f_u [Mpa]	E_s	v_s
329.799	405.056	200000	0.29

2.3. Results of the experiments and discussion

The results of specimens HCFST1, HCFST2, HCFST3, and HCFST4 of HCFST slender columns were previously outlined in Table 1. The axial strength (P_{Test}) of each specimen was determined, along with the relationships between the loads and lateral displacement, axial shortening, vertical strain, and horizontal strain. The mode of failure for each column specimen was also discussed. Based on the experimental tests, the peak axial strength ($P_{ul,Test}$) of the tested columns HCFST1, HCFST2, HCFST3, and HCFST4 was 771.63 kN, 1023.57 kN, 879.75 kN, and 1100.07 kN, respectively. Additionally, the axial shortening at the peak strength was recorded as 6.69, 11.86, 10.12, and 10.06 mm, respectively.

The average load-axial shortening relationships of HCFST slender columns are described in Fig. 9. The current results prove that the shortening values increase with increasing load values. Furthermore, an increase in the columns' cross-sectional dimensions results in higher ultimate load values for HCFST-slender columns. However, it was seen that shortening the height of HCFST slender columns also contributes to an escalation in the ultimate load values.

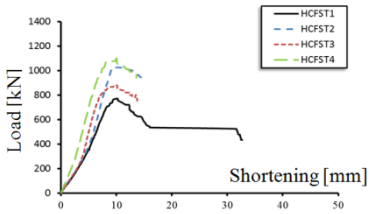

Fig. 9 Load-axial shortening relationships average of LVDT1 and LVDT2 for HCFST

The load- horizontal displacement relationships of the HCFST slender columns are depicted in Fig. 10. It was observed that the load values increased with the lateral displacement values. Additionally, increasing the cross-sectional dimensions of the HCFST slender columns' resulted in higher ultimate load values. Moreover, decreasing the height of the HCFST's slender columns increases the ultimate load. At the middle height of the HCFST slender columns, load-vertical strain and load-horizontal strain were measured and plotted in Fig. 11.

Tension and compression strains were considered positive and negative signs, respectively. The vertical compressive strain and horizontal tension strain of the HCFST slender columns were observed to be greater than the yield strains of their constituent materials ($P_{ul,Test}$). Alternatively, once the vertical strain of the HCFST slender columns (HCFST1, HCFST2, and HCFST3) reversed from compression to tension, the ultimate axial load was determined. Conversely, when attaining the peak load of the HCFST slender columns (HCFST1, HCFST2, and HCFST3), the horizontal strain of the columns was located within the compression zone. Additionally, significant variations in the vertical and horizontal strains of HCFST4 were observed during the initial loading period, due to elastic buckling induced by the slender column. The distorted shapes of the tested columns are depicted in Fig. 12. The failure pattern for the current HCFST slender columns was identified as global buckling, which was typically observed in all columns, particularly in column HCFST1. However, the details of the global buckling behavior of all types of slender columns are illustrated in Fig. 12.

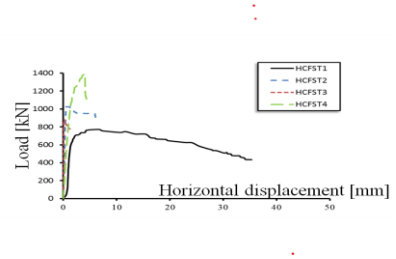

Fig. 10 Load- horizontal displacement relationship average of LVDT3 and LVDT4 for HCFST

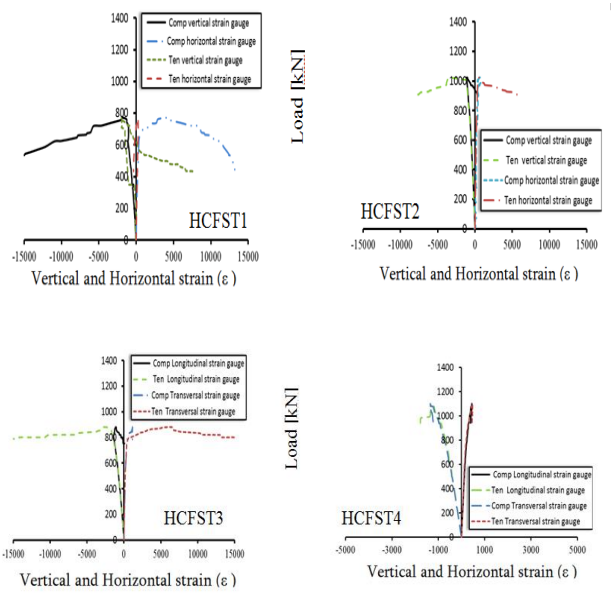

Fig. 11 Load-vertical strain and load-horizontal strain relationships for HCFST slender columns

Fig. 12 Distorted shape of HCFST slender columns

3. Finite element model [FE]

3.1. Overall

The program ABAQUS [32] was utilized to develop the present FE models.

The modeling procedure comprised two steps. Initially, the buckling mode of a perfectly slender column was determined using an elastic buckling analysis referred to as a linear perturbation analysis. In the next stage of the analysis, the HCFST slender columns were loaded through axial compression, determining the peak loads and collapse manner. This analysis incorporated material plasticity strains and geometric imperfections in accordance with the first Eigen mode; RIKS method described in ABAQUS [32]. The model included discrete, rigid upper and lower-end plates, each equipped with a reference point (RP) positioned mid center. These RP's were provided with the boundary conditions, with the vertical load concentrated atop the upper-end plate. Various restrictions were applied at the RPs to simulate pin-ended supports. The lower RP exhibited restraints (u_x= u_y= u_z= θ_z = 0.0), while the top RP exhibited restraints (u_x= u_y= θ_z = 0.0), as shown in Fig. 13 and previously discussed in detail by the first author in [33]. Furthermore, the optimal mesh size was determined through mesh sensitivity analysis, yielding a mesh size of 50mm, as depicted in Fig. 14. The tube was modeled using the shell element with a three-node triangular shape S3 [32]. The concrete was modeled using the three-dimensional solid element C3D4, with a four-node linear tetrahedron shape [32]. Surface-based interactions were used to replicate the interaction between the tube and the concrete. This was achieved using a Coulomb friction model in the tangential orientation on the surface, coupled with a contact pressure-over-closure model in the normal orientation. The steel and concrete surfaces were designated as slave and master surfaces, respectively. As reported by Hassanein et al. [34], the friction coefficient between concrete and steel tube was identified as 0.4. Furthermore, the interaction between the end plates and the concrete was considered to possess the same properties as described above. Additionally, as shown in Fig. 13, all end plates were connected to the tube using the "tie" constraint, as defined in ABAQUS [32]. The stress-strain material of carbon steel was modeled as having bilinear relationships, using the yield and peak strength of steel along with linear strain hardening characterized by a modulus of 2 GPa. Further details on this topic were discussed in the work of the first author [35]. Concrete damage plasticity, available in ABAQUS [32], was selected to simulate the behavior of concrete infill in HCFST slender columns. The full details regarding the stress-strain curve relationships of the infill concrete were provided in [8].

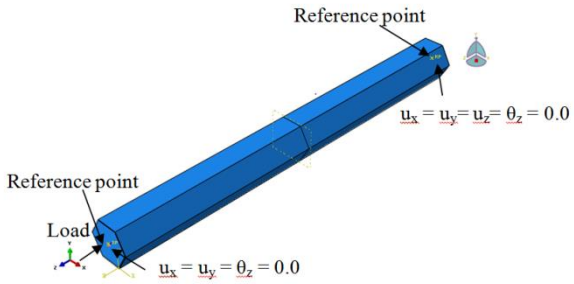

Fig. 13 Load and end conditions on HCFST slender columns

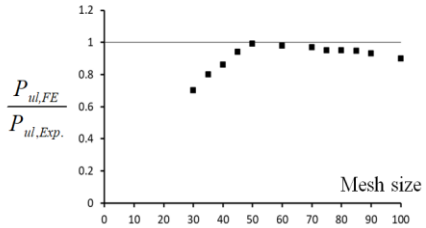

Fig. 14 Mesh sensitivity analysis of HCFST slender columns

3.2. Validation

The FE model was verified using the current HCFST slender columns experimental investigation. Other tests were used to verify the FE from previous research [29, 36].

3.2.1. Validation of the FE model using present tests

The experimental and the FE results were compared concerning ultimate axial load, load-lateral displacement relationships, load-vertical strain relationships, and load-horizontal strain relationships. The ultimate axial strength of the experimental (P_{uExp}) and FE (P_{uEF}) results is compared in Table 5. It is noteworthy that the average value of (P_{uEF}/P_{uExp}) was 0.98, with a standard deviation of (P_{uEF}/P_{uExp}) of 0.038. Therefore, the FE analysis accurately predicted the experimental results for ultimate strength. Additionally, Table 5 compares the strength of FE with the predictions of EC4 (P_{EC4}) and AISC (P_{AISC}), which will be discussed in Section 5.1.3. A comparison of the axial load against horizontal displacement relationships was also made, as shown in Fig. 15. It was observed that the FE model closely aligned with the tested results, accurately including the overall behavior of the axial load-lateral displacement curves, the initial stiffness, and the ultimate axial load. Further comparison was conducted between the axial load against vertical strain and the load against horizontal strain measured at the middle height position on both the tension and compression sides of the column; see Fig. 16. It can be noted that the FE results for vertical and horizontal strain closely matched the tested results; initial stiffness, ultimate load, and overall curve behavior. According to the experimental results, the mode of failure was identified as global buckling; see Fig. 17.

Table 5
Comparison of experimental, FE, and design methods for slender column

S Exp.	P_{uExp}[KN]	P_{uFE}	P_{EC4}[KN]	P_{AISC}[KN]	P_{uFE}	P_{Ec4} /P_{uExp}	P_{AISC}/P_{uExp}
HCFST1	772	774	586	517	1.00	0.76	0.67
HCFST1	1024	1015	917	873	0.99	0.90	0.85
HCFST1	880	862	586	546	0.98	0.67	0.62
HCFST1	1100	1052	917	843	0.96	0.83	0.74
Mean					0.98	0.79	0.72
Deviation from the mean					0.038	0.098	0.099

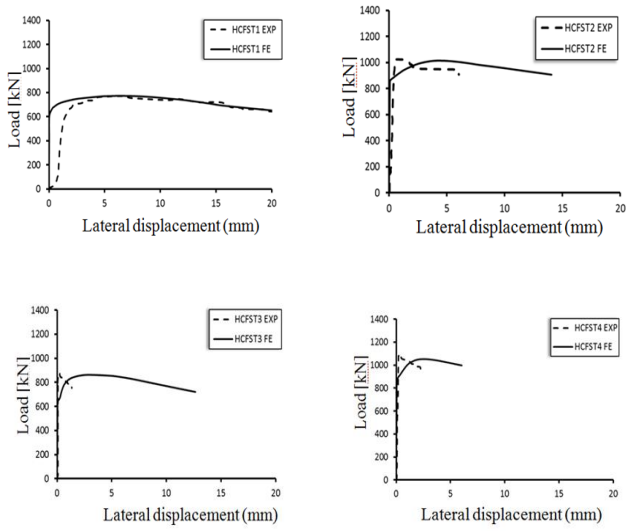

Fig. 15 load-lateral displacement relationship for HCFST slender columns

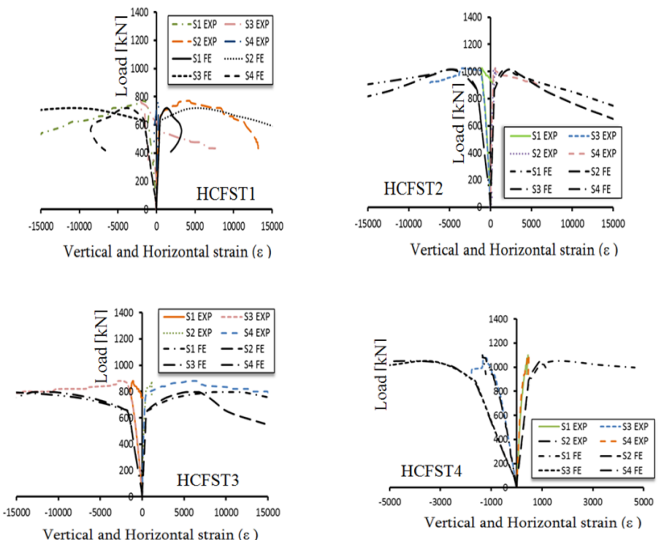

Fig. 16 Load-vertical strain and load-horizontal strain relationships for HCFST

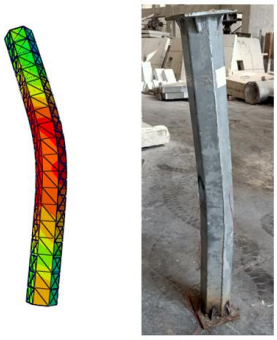

Fig. 17 Mode of failure FE and test results for the HCFST1 slender column specimen

3.2.2. Verification of results: FE and Reference [29]

The FE was validated using the experimental results from reference [29]. Three CFST slender hexagonal column specimens were used in this validation, all sharing sectional dimensions (B = 100 mm and t = 3.95 mm); see Fig. 18. Table 6 presents the geometric properties (B, t, height of column H, θ) and material properties (steel yield strength (f_{y}) and cubic strength of concrete (f_{cu})) listed.

Comparison with the testing results, including experimental axial strength (P_{uExp}), FE axial strength (P_{uFE}), and (P_{uFE}/ P_{uExp}), is depicted in Table 6. The arithmetic mean of (P_{uFE}/ P_{uExp}) was 0.93, with a deviation from the mean of 0.05, indicating a close alignment between the FE experimental axial strengths. Fig. 19 presents another comparison of the axial load against lateral deflection relationships at middle height. Consequently, the FE model accurately predicted the experimental results by accounting for the overall behavior of columns, lateral deflection curves, initial stiffness, and ultimate load.

Table 6
Dimensions and experimental and FE results for HCFST slender columns

S Exp.	B[mm]	t[mm]	H[mm]	f_{cu}[MPa]	f_y	P_{uExp}	P_{uFE}	P_{uFE} /P_{uExp}
HCFT1-0a	100	3.95	1500	89	278.7	2282.8	2004.9	0.88
HCFT1-0b	100	3.95	1500	89	278.7	2052.4	2004.9	0.98
HCFT3-0	100	3.95	2000	89	278.7	2357.6	2158.2	0.92
Mean								0.93
Deviation from the mean								0.05

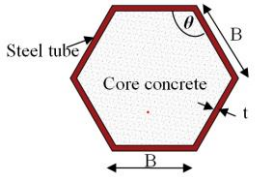

Fig. 18 Dimension of HCFST Ref [29]

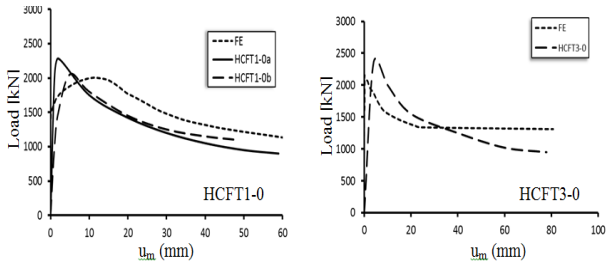

Fig. 19 Axial load–Lateral deflection at mid-height curve for specimens Ref [29]

3.2.3. Validation of the results: FE and Reference [36]

The FE was validated using the experimental results provided in reference [36]. Nine CFST slender circular columns [36] were used, with all specimens having a sectional diameter of (D = 108 mm and t = 4.5 mm), with different values of effective lengths [L_e] and slenderness ratios [λ], as detailed in Table 7. Additionally, the material characteristics (steel yield strength (f_y) and compressive strength of concrete (f_c')) were listed in Table 7. The correspondence between the experimental strength (P_{uExp}) and the FE strength (P_{uFE}) is illustrated in Table 7. The average value of (P_{uFE}/ P_{uExp}) was 0.98, with a deviation from the mean of 0.07, indicating a close match between the FE ultimate load and the experimental results. A comparison of the axial load against lateral displacement relationships at middle height is illustrated in Fig. 20. Consequently, the FE model demonstrated a close correspondence with the experimental results concerning the overall behavior of columns, lateral displacement curves, initial stiffness, and ultimate load.

The FE model yielded satisfactory results concerning the experimental data of the slender concrete-filled columns mentioned above. Consequently, the FE model of HCFST slender columns could be used to simulate the next parametric study.

Table 7
Details and comparison of experimental and FE results Ref. [36]

S Exp.	D[mm]	t[mm]	L_e[mm]	f_c[MPa]	f_y	P_{uExp}	P_{uFE}	P_{uFE} /P_{uExp}
sc154-3	108	4.5	4158	37.4	348	298	291	0.98
sc154-4	108	4.5	4158	37.4	348	280	291	1.04
sc149-1	108	4.5	4023	37.4	348	318	297	0.94
sc149-2	108	4.5	4023	37.4	348	320	297	0.93
sc141-1	108	4.5	3807	25.4	348	350	377	1.07
sc141-2	108	4.5	3807	25.4	348	370	377	1.02
sc130-1	108	4.5	3510	25.4	348	400	396	0.99
sc130-2	108	4.5	3510	25.4	348	390	396	1.02
sc130-3	108	4.5	3510	37.4	348	440	364	0.83
Mean								0.98
Deviation from the mean								0.07

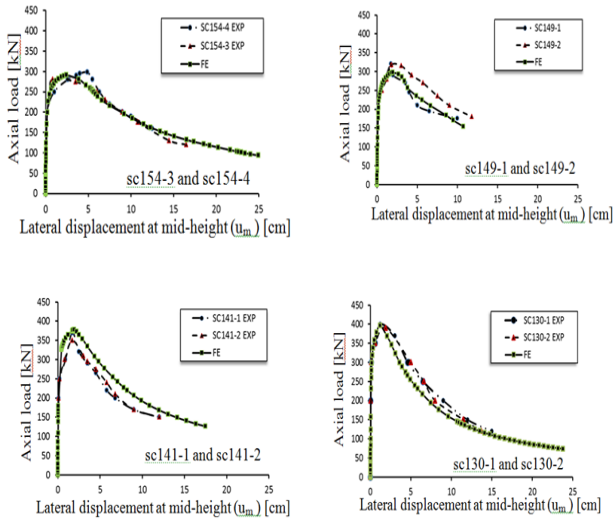

Fig. 20 Axial load–Lateral displacement at mid-height curve for specimens Ref [36]

4. Parametric study

In this part, a parametric study was conducted to simulate the behavior of HCFST slender columns utilizing the model described in the preceding section. The variables of the parametric study were the steel's cross-section (D × B), steel's cross-sectional thickness (t), height of HCFST slender columns (H), (θ of the cross-section 120º), (a = $D/2$) and slenderness ration (λ), as detailed in Tables 8 and 9. Additionally, Tables 8 and 9 presented the details on the steel columns' yield, ultimate (f_y *and* f_u), nominal compression strength of concrete, and the peak load of the FE P_{ulFE}. In this study, an initial imperfection of ($L/1000$) was considered. Young's modulus and Poison's ratio of E_s = 200 GPa and ν_s = 0.3 were respectively adopted and used.

4.1. Slenderness ratio (λ)

The steel cross-section of dimensions D × B × t (600 × 519.62 × 6mm), yield (f_y) and ultimate (f_u) strengths of the steel columns (275 and 430 MPa, respectively), and the nominal compression strength of concrete (f_c = 25

MPa) were examined in this study. Examinations were conducted across various column slenderness ratios (λ) ranging from 7.30 to 182.60, as detailed in Table 8. Therefore, a comprehensive comparison was made between very long columns that failed owing to elastic buckling and short-height columns that failed owing to inelastic buckling. The relationship between peak axial strength (P_{ulFE}) and the cross-sectional strength ($P_{Hassanein}$) [8] for different slenderness ratios (λ) is depicted in Fig. 21.

$$P_{Hassanein}=(\gamma_c f'_c+4.1 f_{rp})A_c+f_y A_s \quad (1)$$

$$f_{rp}=\begin{cases}\left(0.0491703-0.000794\frac{B+D}{2t}\right)f_{sy} & for\ 17\le\frac{B+D}{2t}<63\\ \left(0.0065311-0.0000044\frac{B+D}{2t}\right)f_{sy} & for\ 63\le\frac{B+D}{2t}\le103\end{cases} \quad (2)$$

Where A_s was a steel section area, A_c was a concrete section area, and factor, f_{rp}, was the confinement pressure of regular HCFST.

$$\lambda_{EC4}=\frac{L_e}{\sqrt{I_{DS}/A_{DS}}}\ [37] \quad (3)$$

Where L_e was the length of the effective buckling, I_{DS} was the HCFST column section's moment of inertia, and A_{DS} was the HCFST's cross-sectional area.

Fig. 21 illustrates that as the value of (λ) increased, the peak axial strength of the HCFST column decreased. Additionally, it was observed that the maximum value of λ, which describes the limit for short HCFST columns was, approximately 18. Beyond this limit, the columns were considered slender.

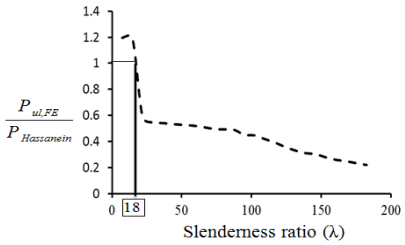

Fig. 21 Variation of the slenderness ratio (λ) with the HCFST's relative capacities

4.2. The thickness (t)

In this part, the effect of steel tube thickness (t) was studied. $D \times B$ (300 × 259.81mm) with f_y = (235, 275, 355 MPa), f_u = (360, 430, 510 MPa), f_c = (30, 40 MPa), and a height of (3000, 4000, 5000, 6000mm) were used.

Fig. 22 illustrates the relationship between lateral displacement and axial load. Generally, the peak axial load decreased as the thickness (t) of the steel tube decreased. It was observed that all curves exhibited the same trend. It is noteworthy that increasing the thickness of the steel cross-section led to an increase in the peak load for HCFST. As shown in Table 9, increasing the height of the HCFST resulted in a reduction of the peak axial load. The effect of increasing the thickness of the steel tube (t) distinctly influenced the enhancement of axial strength for shorter-height columns compared to longer-height columns. Therefore, it is recommended to increase the thickness of the tube section at short and medium heights.

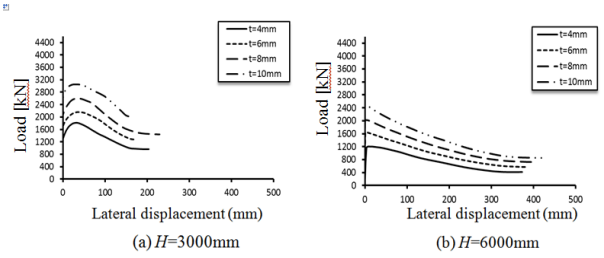

Fig. 22 Load- Lateral displacement relationship for HCFST in case f_y= 235MPa and f_c= 30MPa

4.3. Strength of steel (fy)

In this part, the influence of steel's strength [f_y] was studied. $D \times B$ (300 × 259.81mm) with [t] (4, 6, 8, 10mm), f_c = (30, 40 MPa), and a height of (3000, 4000, 5000, 6000mm) were used.

The peak axial load results for the HCFST slender columns' were presented in Fig. 23. Generally, it was observed that the peak axial load increased with increasing values of [f_y]. As shown in Table 9, increasing the height of the HCFST led to a reduction in the peak load. It was deduced from Table 9 that there was an average increase of approximately 15% in the ultimate axial load with an increase in yield strength.

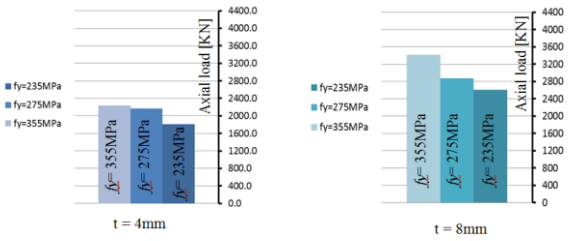

Fig. 23 Comparison of ultimate axial load for HCFST slender columns in case of; (H=3000mm and f_c= 30MPa)

4.4. Concrete strength (f_c)

In this part, the influence of concrete strength (f_c) was studied. $D \times B$ (300 × 259.81mm) with t = (4, 6, 8, 10mm), f_y = (235, 275,355 MPa), f_u = (360, 430,510 MPa) and a height of (3000, 4000, 5000, 6000mm) were used.

Fig. 24 presents the peak axial load results for the HCFST slender columns'. Generally, an increase in the steel cross-section's thickness (t) correlates with an increase in the peak axial load for HCFST slender columns. It is noteworthy that the peak axial load increases with increasing values of f_c, as illustrated in Table 9. Moreover, increasing the height of the HCFST leads to a decrease in the peak load. In reference to Fig. 24 and the results illustrated in Table 9, it is evident that the increase in peak load is clearly observed in the short-height column and could be disregarded in the long-height column regardless of changes in tube thickness. Therefore, it is recommended that in normal concrete, there is no need to increase the concrete strength (f_c).

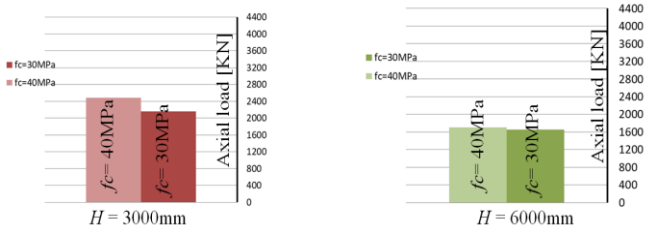

Fig. 24 Comparison of ultimate axial load for HCFST slender columns in case of; (t=6mm and f_y = 235MPa)

4.5. The height (H)

This part studied the impact of height (H). $D \times B$ (300 × 259.81mm) with f_y (235, 275,355 MPa), f_u (360, 430,510 MPa), respectively f_c (30, 40 MPa), and t (4, 6, 8, 10mm) were studied.

Fig. 25 depicts the relationship between axial load and lateral displacement. Generally, the peak load of HCFST slender columns' decreased as the height of HCFST increased. However, the decreases in the short-height column were large compared to the long-height column. The results indicate that the peak load for HCFST increased as the thickness of the steel cross-section increased, as indicated in Table 9.

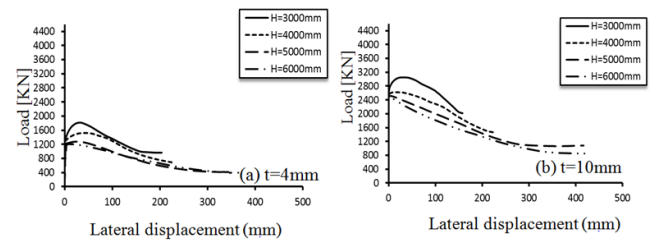

Fig. 25 Load- Lateral displacement relationship for HCFST in case f_y= 235MPa and f_c= 30MPa

Table 8
Slenderness of the HCFST columns

Column	H[mm]	$D[mm]$	$B[mm]$	t[mm]	a [mm]	f_y[MPa]	f_c[MPa]	λ	P_{uFE}[KN]
HC1	1000	600	519.62	6	300	275	25	7.30	7684
HC2	2000	600	519.62	6	300	275	25	14.60	7685
HC3	3000	600	519.62	6	300	275	25	21.90	3777
HC4	4000	600	519.62	6	300	275	25	29.20	3513
HC5	5000	600	519.62	6	300	275	25	36.50	3480
HC6	6000	600	519.62	6	300	275	25	43.80	3426
HC7	7000	600	519.62	6	300	275	25	51.10	3390
HC8	8000	600	519.62	6	300	275	25	58.40	3352
HC9	9000	600	519.62	6	300	275	25	65.70	3280
HC10	10000	600	519.62	6	300	275	25	73.00	3188
HC11	11000	600	519.62	6	300	275	25	80.30	3170
HC12	12000	600	519.62	6	300	275	25	87.60	3148
HC13	13000	600	519.62	6	300	275	25	94.90	2900
HC14	14000	600	519.62	6	300	275	25	102.20	2873
HC15	15000	600	519.62	6	300	275	25	109.50	2690
HC16	16000	600	519.62	6	300	275	25	116.85	2524
HC17	17000	600	519.62	6	300	275	25	124.15	2300
HC18	18000	600	519.62	6	300	275	25	131.45	2128
HC19	19000	600	519.62	6	300	275	25	138.75	2000
HC20	20000	600	519.62	6	300	275	25	146.00	1948
HC21	21000	600	519.62	6	300	275	25	153.35	1789
HC22	22000	600	519.62	6	300	275	25	160.65	1668
HC23	23000	600	519.62	6	300	275	25	168.00	1599
HC24	24000	600	519.62	6	300	275	25	175.30	1501
HC25	25000	600	519.62	6	300	275	25	182.60	1414

Table 9
Comparison between FE results and design methods of slender columns

Column	H[mm]	$t[mm]$	$f_y[MPa]$	$f_c[MPa]$	$P_{uFE}[KN]$	P_{Ec4}KN]	P_{AISC}[KN]	P_{Ec4} / P_{uFE}	P_{AISC} / P_{uFE}
C1	3000	4	235	30	1814	1539	1372	0.85	0.77
C2	3000	6	235	30	2161	1533	1368	0.71	0.63
C3	3000	8	235	30	2603	1528	1364	0.59	0.52
C4	3000	10	235	30	3052	1523	1360	0.50	0.45
C5	4000	4	235	30	1524	1539	1271	1.01	0.83
C6	4000	6	235	30	1887	1533	1267	0.81	0.67
C7	4000	8	235	30	2185	1528	1263	0.70	0.58
C8	4000	10	235	30	2624	1523	1259	0.58	0.48
C9	5000	4	235	30	1277	1538	1152	1.20	0.90
C10	5000	6	235	30	1694	1533	1148	0.91	0.68
C11	5000	8	235	30	2100	1528	1145	0.73	0.55
C12	5000	10	235	30	2515	1523	1141	0.61	0.45
C13	6000	4	235	30	1205	1538	1022	1.28	0.85
C14	6000	6	235	30	1650	1533	1018	0.93	0.62
C15	6000	8	235	30	2023	1528	1015	0.76	0.50
C16	6000	10	235	30	2478	1523	1011	0.61	0.41
C17	3000	4	275	30	2232	1772	1560	0.80	0.70
C18	3000	6	275	30	2484	1767	1556	0.71	0.63
C19	3000	8	275	30	2875	1762	1551	0.61	0.54
C20	3000	10	275	30	3224	1757	1548	0.55	0.48
C21	4000	4	275	30	1686	1772	1428	1.05	0.85
C22	4000	6	275	30	2094	1767	1424	0.84	0.68

C23	4000	8	275	30	2466	1762	1420	0.71	0.58
C24	4000	10	275	30	3021	1757	1416	0.58	0.47
C25	5000	4	275	30	1476	1772	1275	1.20	0.86
C26	5000	6	275	30	1984	1767	1271	0.89	0.64
C27	5000	8	275	30	2463	1762	1267	0.72	0.51
C28	5000	10	275	30	2936	1757	1264	0.60	0.43
C29	6000	4	275	30	1429	1772	1110	1.24	0.78
C30	6000	6	275	30	1899	1767	1106	0.93	0.58
C31	6000	8	275	30	2347	1762	1103	0.75	0.47
C32	6000	10	275	30	2879	1757	1099	0.61	0.38
C33	3000	4	355	30	2468	2240	1918	0.91	0.78
C34	3000	6	355	30	2884	2235	1914	0.77	0.66
C35	3000	8	355	30	3413	2230	1910	0.65	0.56
C36	3000	10	355	30	3747	2225	1905	0.60	0.51
C37	4000	4	355	30	2110	2240	1715	1.06	0.81
C38	4000	6	355	30	2580	2235	1711	0.87	0.66
C39	4000	8	355	30	3201	2230	1707	0.70	0.53
C40	4000	10	355	30	3618	2225	1702	0.61	0.47
C41	5000	4	355	30	1946	2240	1485	1.15	0.76
C42	5000	6	355	30	2437	2235	1481	0.92	0.61
C43	5000	8	355	30	3066	2230	1477	0.73	0.48
C44	5000	10	355	30	3609	2225	1473	0.62	0.41
C45	6000	4	355	30	1697	2240	1246	1.32	0.73
C46	6000	6	355	30	2361	2235	1242	0.95	0.53
C47	6000	8	355	30	2746	2230	1238	0.81	0.45
C48	6000	10	355	30	3175	2225	1234	0.70	0.39
C49	3000	4	235	40	2076	1593	1411	0.77	0.68
C50	3000	6	235	40	2489	1586	1406	0.64	0.56
C51	3000	8	235	40	2990	1580	1400	0.53	0.47
C52	3000	10	235	40	3301	1573	1395	0.48	0.42
C53	4000	4	235	40	1818	1593	1305	0.88	0.72
C54	4000	6	235	40	2016	1586	1300	0.79	0.64
C55	4000	8	235	40	2456	1580	1295	0.65	0.53
C56	4000	10	235	40	2656	1573	1290	0.60	0.49
C57	5000	4	235	40	1410	1593	1180	1.13	0.84
C58	5000	6	235	40	1804	1586	1175	0.88	0.65
C59	5000	8	235	40	2181	1580	1171	0.72	0.54
C60	5000	10	235	40	2577	1573	1166	0.61	0.45
C61	6000	4	235	40	1289	1593	1044	1.24	0.81
C62	6000	6	235	40	1701	1586	1039	0.93	0.61
C63	6000	8	235	40	2080	1580	1035	0.82	0.55
C64	6000	10	235	40	2209	1573	1031	0.71	0.47
C65	3000	4	275	40	2273	1827	1598	0.80	0.70
C66	3000	6	275	40	2648	1820	1593	0.69	0.60
C67	3000	8	275	40	3193	1813	1587	0.57	0.50
C68	3000	10	275	40	3479	1807	1582	0.52	0.45
C69	4000	4	275	40	2023	1827	1461	0.90	0.72
C70	4000	6	275	40	2245	1820	1456	0.81	0.65
C71	4000	8	275	40	2577	1813	1451	0.70	0.56
C72	4000	10	275	40	3115	1807	1446	0.58	0.46
C73	5000	4	275	40	1727	1827	1301	1.06	0.75
C74	5000	6	275	40	2027	1820	1296	0.90	0.64
C75	5000	8	275	40	2489	1813	1292	0.73	0.52

C76	5000	10	275	40	2988	1807	1287	0.60	0.43
C77	6000	4	275	40	1439	1827	1130	1.27	0.79
C78	6000	6	275	40	1963	1820	1125	0.93	0.57
C79	6000	8	275	40	2429	1813	1121	0.75	0.46
C80	6000	10	275	40	2963	1807	1117	0.61	0.38
C81	3000	4	355	40	2543	2295	1955	0.90	0.77
C82	3000	6	355	40	3122	2288	1949	0.90	0.62
C83	3000	8	355	40	3729	2281	1944	0.73	0.52
C84	3000	10	355	40	4222	2274	1938	0.61	0.46
C85	4000	4	355	40	2270	2295	1745	1.01	0.77
C86	4000	6	355	40	2750	2288	1740	0.83	0.63
C87	4000	8	355	40	3312	2281	1735	0.69	0.52
C88	4000	10	355	40	3665	2274	1729	0.62	0.47
C89	5000	4	355	40	1909	2295	1509	1.59	1.05
C90	5000	6	355	40	2575	2288	1503	1.17	0.77
C91	5000	8	355	40	3148	2281	1498	0.94	0.62
C92	5000	10	355	40	3473	2274	1493	0.77	0.50
C93	6000	4	355	40	1746	2295	1262	1.31	0.72
C94	6000	6	355	40	2446	2288	1258	0.94	0.51
C95	6000	8	355	40	2745	2281	1253	0.83	0.46
C96	6000	10	355	40	3210	2274	1249	0.71	0.39
Mean								0.81	0.60
Standard deviation								0.22	0.14

5. Design methods

5.1. Available design methods

In this part, available design strength methods for CFST slender columns were discussed in the case of compact cross-sections.

5.1.1. EN 1994-1-1(EC4) [37]

For a CFST column's ultimate axial capacity, used the EN 1994-1-1 (EC4) [37] equation (P_{EC4}) as known by Eq. (4).

$$P_{Ec4}=\chi P_{pl,Rd} \tag{4}$$

Where $P_{pl,Rd}$ was the plastic strength to axial compression with consideration for the confinement concrete when the ratio of slenderness (λ) did not exceed 0.5, as seen in the following:

$$P_{pl,Rd}=\begin{cases} A_c f'_c(1+\eta_a \frac{t}{D}\frac{f_y}{f'_c})+A_s f_y & : \lambda' \le 0.5 \\ A_c f'_c + A_s f_y & : \lambda' > 0.5 \end{cases} \tag{5}$$

$$\eta_a=0.25(3+2\lambda') \le 1.0 \tag{6}$$

$$\eta_c = 4.9 - 18.5\lambda' + 17\lambda'^2 \ge 0 \tag{7}$$

$$\lambda'=\sqrt{\frac{P_{pl,Rd}(6.30)}{P_{cr}}} \tag{8}$$

$$P_{pl,Rd}(6.30)=0.85 f_c A_c + f_y A_s \tag{9}$$

$$P_{cr}=\frac{\pi^2 (EI_{eff})}{(L_e)^2} \tag{10}$$

$$EI_{eff}=E_s I_s + k_e E_c I_c \tag{11}$$

$k_e = 0.6$

Where (EI_{eff}) was the effective elastic flexural stiffness, L_e was the element's effective height, P_{cr} was the elastic critical buckling, and k_e was a correction factor.The reduction factor (χ) was:

$$\chi=\frac{1}{(\phi+\sqrt{\phi^2-\lambda'^2})} \le 1.0 \tag{12}$$

$$\phi=0.5(1+\alpha(\lambda'-\lambda'_0)+\lambda'^2) \tag{13}$$

$\alpha = 0.34$

$\lambda'_o=0.2$

5.1.2. AISC specification [38]

Provided the equation for a CFST column's ultimate axial capacity (P_{AISC}) by the AISC specification [38] Eq. (14).

$$P_{AISC}=\begin{cases} P_{no}\left[0.658^{(P_{no}/P_e)}\right] & : \frac{P_{no}}{P_e} \le 2.25 \\ 0.877 P_e & : \frac{P_{no}}{P_e} > 2.25 \end{cases} \tag{14}$$

$$P_{no}=0.85 A_c f'_c + A_s f_y \tag{15}$$

$$EI_{eff}=E_s I_s + C_1 E_c I_c$$

C1 = 0.7

5.1.3. Comparison and discussion

In this section, an initial comparison was conducted between the peak design strength of square CFST slender columns and the experimentally determined peak strength of HCFST slender columns, as explained in Section 2.3. Table 5 displays a comparison of the experimental results with the peak load calculated by EC4 and AISC. The average peak load ratio of the P_{EC4} [37] to the experimental (P_{Ec4}/P_{uExp}) was 0.79, with a deviation from the mean of 0.098. Additionally, the ratio of P_{AISC} [38] to the experimental (P_{AISC}/P_{uExp}) had mean of 0.72, with a standard deviation of 0.099. Secondly, comparisons were made between the peak design strength of square CFST slender columns and the parametric study conducted using the FE model of HCFST slender columns. Table 9 displays a comparison of the FE results with the ultimate load as determined by EC4 and AISC. The average peak load ratio of the P_{EC4} [37] and FE results (P_{Ec4}/P_{uExp}) was 0.81, with a standard deviation of 0.22. Similarly, the average ultimate load ratio between the P_{AISC} [38] and the FE results (P_{AISC}/P_{uExp}) was 0.60, with a deviation from the mean of 0.14. Based on the results in Tables 5 and 9, it was observed that the design strength derived from the EN 1994-1-1 (EC4) design method gave unconservative results for smaller thicknesses (4mm) of steel tubes, while it provided conservative results for larger thicknesses of steel tubes in HCFST slender columns. Conversely, the AISC specification yielded conservative results across all thicknesses of steel tubes for HCFST slender columns. From the previous comparison, it was concluded that AISC can be used for tubes with small thicknesses up to 4mm, while EC4 is suitable for tubes with thicknesses above 4mm.

6. Conclusions

An experimental and FE model investigation of axially loaded HCFST slender columns has been provided in this paper. The experiments and the FE model aim to study the impact of both the cross-section and concrete strength on the strength and behavior of HCFST slender columns.

Building upon the present experimental results and FE model investigations, the following conclusions could be drawn:

1. It is noted that the ultimate load values for hexagonal slender columns increased with the increase in cross- sectional dimensions. However, it was observed that reducing the height of HCFST slender columns led to an increase in ultimate load values.

2. The mode of failure observed in the present HCFST slender columns was predominantly global buckling, a phenomenon consistently observed for all columns, particularly in column HCFST1.

3. The experimental results provided a reliable prediction of the FE model's peak axial strength. The observed mode of failure, consistent with the experimental results, was global buckling.

4. It was determined that the maximum value of λ, representing the limit of short HCFST columns, was approximately 18. Beyond this limit, the columns were considered slender.

5. The peak axial load for HCFST slender columns increased as the values of (t, f_c, and f_y) increased.

6. Increasing the thickness of the steel tube (t) had a clear effect on enhancing the axial strength of shorter-height columns compared to longer-height columns. Consequently, it is recommended to increase the thickness of the tube section at short and medium heights.

7. It is noted that there was an average increase of approximately 15% in the peak axial load associated with an increase in yield strength.

8. It was observed that the increase in peak axial load was clearly evident in the short-height column and could be disregarded in the long-height column, irrespective of changes in tube thickness. Therefore, it can be recommended that there is no need to increase the concrete's strength (f_c) in normal concrete.

9. It was observed that the design strength based on the EC4 design method yielded unconservative results for smaller thicknesses (4mm) of steel tubes while providing conservative results for larger thicknesses of steel tubes in HCFST slender columns. Conversely, the AISC specification yielded conservative results across all thicknesses of steel tubes for HCFST slender columns.

Recommendations

1- It is recommended to increase the tube thickness for columns of short and medium heights.
2- It is advisable that in normal concrete, there is no need to increase the concrete's strength (f_c).
3- It is recommended to use the design strength specifications of AISC for tubes with thicknesses up to 4mm and EC4 for tubes with other thicknesses.

Finally, it is recommended to conduct additional experimental tests to examine the analysis of HCFST slender columns using high-strength concrete and steel with various cross-sections.

References

[1] Xu W, Han L-H, Li W. " Performance of hexagonal CFST members under axial compression and bending" , J Constr Steel Res Vol. 123, pp. 162–175, 2016.
[2] Sakino K, Nakahara H, Morino S, and Nishiyama I. "Behavior of centrally loaded concrete-filled steel-tube short columns", Journal of Structural Engineering Vol. 130(2), pp. 180-188, 2004.
[3] Ding F-X, Li Z, Cheng S, and Yu Z-W. "Composite action of octagonal concrete-filled steel tubular stub columns under axial loading", Thin-Walled Structures Vol.107, pp.453-461,2016.
[4] Hassanein MF, Patel VI, Elchalakani M, and Thai H-T. "Finite element analysis of large diameter high strength octagonal CFST short columns", Thin-Walled Structures Vol.123, pp.467-482, 2018.
[5] Zhu J-Y and Chan T-M. "Experimental investigation on octagonal concrete filled steel stub columns under uniaxial compression', Journal of constructional steel research. Vol.147, pp.457-467, 2018.
[6] Ahmed M and Liang QQ. "Numerical modeling of octagonal concrete-filled steel tubular short columns accounting for confinement effects", Engineering Structures Vol.226, pp.111405,2020.
[7] Ding F-X, Li Z, Cheng S, and Yu Z-W. "Composite action of hexagonal concrete-filled steel tubular stub columns under axial loading", Thin-Walled Structures Vol.107, pp.502-513,2016.
[8] Hassanein, M.F., Patel, V.I., and Bock, M.," Behaviour and design of hexagonal concrete-filled steel tubular short columns under axial compression ", Engineering Structures, Vol. 153, pp. 732-748, 2017
[9] Liu J, Li Z, and Ding F-X. "Experimental Investigation on the Axially Loaded Performance of Notched Hexagonal Concrete-Filled Steel Tube (CFST) Column" Advances in Civil Engineering; Vol.2612536, 2019.
[10] Ahmed M and Liang QQ. "Numerical analysis of concentrically loaded hexagonal concrete-filled steel tubular short columns incorporating concrete confinement", Advances in Structural Engineering 13694332211004111, 2021.
[11] Wang Z, Chen J, Xie E, and Lin S," Behavior of concrete-filled round-ended steel tubular stub columns under axial compression", Journal of Building Structures Vol. 35(7), pp. 123-130 (Chinese), 2014.
[12] Hassanein MF and Patel VI," Round-ended rectangular concrete-filled steel tubular short columns: FE investigation under axial compression", Journal of Constructional Steel Research Vol.140, pp. 222-236, 2018.
[13] Piquer A, Ibañez C, and Hernández-Figueirido D," Structural response of concrete-filled round-ended stub columns subjected to eccentric loads", Engineering Structures Vol.184, pp. 318-328, 2019.
[14] Ahmed M and Liang QQ. "Numerical analysis of thin-walled round-ended concrete-filled steel tubular short columns including local buckling effects", Structures Vol.28, pp. 181-196, 2020.
[15] Ahmed M, Ci J, Yan X-F, and Chen S. "Nonlinear analysis of elliptical concrete-filled stainless steel tubular short columns under axial compression", Structures Vol.32, pp. 1374-1385, 2021.
[16] Ahmed M and Liang QQ. "Computational simulation of elliptical concrete-filled steel tubular short columns including new confinement model". Journal of Constructional Steel Research, Vol.174, pp. 106294, 2020.
[17] Cai Y, Quach W-M, and Young B. "Experimental and numerical investigation of concrete-filled hot-finished and cold-formed steel elliptical tubular stub columns". Thin-Walled Structures, Vol.145, pp. 106437, 2019.
[18] Hassanein MF, Patel VI, El Hadidy AM, Al Abadi H, and Elchalakani M. " Structural behaviour and design of elliptical high-strength concrete-filled steel tubular short compression members", Engineering Structures, Vol.173, pp. 495-511, 2018.
[19] Lam D, Gardner L, and Burdett M. "Behaviour of axially loaded concrete filled stainless steel elliptical stub columns. Advances in Structural Engineering", Vol.13(3) , pp. 493-500, 2010 .
[20] Ci J, Chen S, Jia H, Yan W, Song T, and Kim K-S. Axial compression performance analysis and bearing capacity calculation on square concrete-filled double-tube short columns. Marine Structures, Vol.72, pp. 102775, 2020.
[21] Pei WJ, Research on mechanical performance of multibarrel tube-confined concrete columns. Chang'an University, Xian, China, ME Thesis, 2005.
[22] Qian J, Zhang Y, Ji X, and Cao W. Test and analysis of axial compressive behavior of short composite-sectioned high strength concrete filled steel tubular columns. Journal of Building Structures, Vol.32(12) , pp.162-169 (in Chinese), 2011.
[23] Qian J, Zhang Y, and Zhang W. Eccentric compressive behavior of high strength concrete filled double-tube short columns. Journal of Tsinghua University (Science and Technology), Vol.55(1) , pp.1-7 (in Chinese), 2015.
[24] Xiong MX, Xiong DX, and Liew JYR. Behaviour of steel tubular members infilled with ultra high strength concrete. Journal of Constructional Steel Research, Vol.138, pp.168-183, 2017 .
[25] Ahmed M, Liang QQ, Patel VI, and Hadi MNS. Experimental and numerical studies of square concrete-filled double steel tubular short columns under eccentric loading. Engineering Structures, Vol.197, pp.109419, 2019.
[26] Dundu, M., " Column buckling tests of hot-rolled concrete filled square hollow sections of mild to high strength steel" Engineering Structures, Vol. 127, pp. 73-85, 2016.
[27] X.H. Dai, D.Lam, N.Jamaluddin, J.Ye " Numerical analysis of slender elliptical concrete filled columns under axial compression ", Thin-Walled Structures, Vol. 77, pp. 26-35, 2014.
[28] Ahmed M, Liang QQ, Patel VI, and Hadi MNS. "Nonlinear analysis of square concrete-filled double steel tubular slender columns incorporating preload effects". Engineering Structures, Vol.207, pp. 110272, 2020.
[29] Wang, Z.B. , Tao, Z., Yu, Q. , GuoJ-T. "Behavior of hexagonal concrete-filled steel corner columns under eccentric compression", Journal of Constructional Steel Research, Vol. 200, pp. 107659, 2023.
[30] ECP 2001: "Egyptian Code of Practice for Reinforced Concrete Construction", Code No. 203, Cairo, Egypt, 2001.
[31] Australian Standard, "Methods for tensile testing of metals", AS 1391. Sydney, Australia,

Standards Association of Australia, 1991.
[32] ABAQUS Standard, User's Manual The Abaqus Software is a product of Dassault Systèmes Simulia Corp., Providence, RI, USA Dassault Systèmes, Version 6.8,USA, 2008.
[33] Hassanein M.F., Kharoob, O.F.," Analysis of circular concrete-filled double skin tubular slender columns with external stainless steel tubes", Thin-Walled Structures, Vol. 79, pp. 23-37, 2014.
[34] Hassanein M.F., Kharoob, O.F.,Liang, Q.Q.,"Behaviour of circular concrete-filled lean duplex stainless steel–carbon steel tubular short columns" Eng. Struct Vol .56 , pp.83–94, 2013.
[35] Hassanein M.F., Kharoob, O.F., Q.Q. Liang"Circular concrete-filled double skin tubular short columns with external stainless steel tubes under axial compression, Thin-Walled Structures, Vol. 73, pp. 252-263, 2013.
[36] Han, LH., "Tests on concrete filled steel tubular columns with high slenderness ratio", Advances in Structural Engineering, Vol. 3(4), pp. 337-344, 2000.
[37] EN 1994-1-1: Eurocode 4. Design of composite steel and concrete structures. Part 1. 1, general rules and rules for buildings. European Committee for Standardization, 2004
[38] AISC, Specification for Structural Steel Buildings, AISC, Chicago, IL, USA, 2016.